412TW-PA-12950

FLUID STRUCTURE MODELING AND SIMULATION OF A MODIFIED KC-135R ICING TANKER BOOM

Daniel A. Reasor Jr., PhD
Jason A. Lechniak
Keerti K. Bhamidipati
Micah R. Besson
Crystal L. Pasiliao

AIR FORCE TEST CENTER
EDWARDS AFB, CA

7 January 2013

412TW

AIR FORCE TEST CENTER
EDWARDS AIR FORCE BASE, CALIFORNIA
AIR FORCE MATERIEL COMMAND
UNITED STATES AIR FORCE

REPORT DOCUMENTATION PAGE

Form Approved
OMB No. 0704-0188

1. REPORT DATE *(DD-MM-YYYY)*	**2. REPORT TYPE**	**3. DATES COVERED** *(From - To)*
7 January 2013	AIAA Conference Paper 2013-0053	

4. TITLE AND SUBTITLE

Fluid-Structure Modeling and Simulation of a Modified KC-135R Icing Tanker Boom

5a. CONTRACT NUMBER

5b. GRANT NUMBER

5c. PROGRAM ELEMENT NUMBER

6. AUTHOR(S)

Daniel A. Reasor Jr., Jason A. Lechniak, Keerti K. Bhamidipati, Micah R. Besson, Crystal L. Pasiliao

5d. PROJECT NUMBER

5e. TASK NUMBER

5f. WORK UNIT NUMBER

7. PERFORMING ORGANIZATION NAME(S) AND ADDRESS(ES) AND ADDRESS(ES)

412th Test Wing, 812th Test Support Squadron
304 East Popson Avenue Edwards AFB, CA 93524

8. PERFORMING ORGANIZATION REPORT NUMBER

412TW-PA-12950

9. SPONSORING / MONITORING AGENCY NAME(S) AND ADDRESS(ES)

10. SPONSOR/MONITOR'S ACRONYM(S)

N/A

11. SPONSOR/MONITOR'S REPORT NUMBER(S)

12. DISTRIBUTION / AVAILABILITY STATEMENT

Approved for public release A: distribution is unlimited.

13. SUPPLEMENTARY NOTES

CA: Air Force Test Center Edwards AFB CA CC: 012100

14. ABSTRACT

The objective of this study is to build a physics-based computational model of the Airborne Icing Tanker (AIT) boom system to provide an aeroelastic modeling and simulation (M&S) capability to complement flight test. The AIT boom system is a KC-135R aircraft with a modified high-speed aerial refueling tanker boom and icing array. The ground vibration test (GVT) results of the AIT boom system are used to validate a finite element (FE) structural model via comparison of mode shapes and frequencies. An aerodynamic evaluation of two array designs is also presented. This approach can be used to evaluate future array designs and provide array stability information prior to wind-tunnel and flight tests once validated.

15. SUBJECT TERMS

Finite Element, Computational Fluid Dynamics, Ground Vibration Test, Structures, Aerodynamics, Aeroelasticity, Modeling and Simulation

16. SECURITY CLASSIFICATION OF:			**17. LIMITATION OF ABSTRACT**	**18. NUMBER OF PAGES**	**19a. NAME OF RESPONSIBLE PERSON**
Unclassified					412 TENG/EN (Tech Pubs)
a. REPORT	**b. ABSTRACT**	**c. THIS PAGE**			**19b. TELEPHONE NUMBER** *(include area code)*
Unclassified	Unclassified	Unclassified	None	19	661-277-8615

2013-(Control ID:1420821)
51st Aerospace Sciences Meeting including the New Horizons Forum and Aerospace Exposition; Grapevine, TX; 7-10 January 2013

Fluid-Structure Modeling and Simulation of a Modified KC-135R Icing Tanker Boom

Jason A. Lechniak*, Keerti K. Bhamidipati†, Micah R. Besson‡, and Daniel A. Reasor Jr.§
412th Test Wing – Edwards, California 93524 U.S.A.

The objective of this study is to build a physics-based computational model of the Airborne Icing Tanker (AIT) boom system to provide an aeroelastic modeling and simulation (M&S) capability to complement flight test. The AIT boom system is a KC-135R aircraft with a modified high-speed aerial refueling tanker boom and icing array. The ground vibration test (GVT) results of the AIT boom system, used to validate a finite element (FE) structural model via comparison of mode shapes and frequencies prior to use in fluid-structure interaction (FSI) simulations, is presented hererin. An aerodynamic evaluation of two array designs is also presented. This approach can be used to evaluate future array designs and provide array stability information prior to wind-tunnel and future flight tests once validated.

I. Introduction

Benefits of M&S tools include the early discovery of defects, reduced risk through increased knowledge of physical phenomena, and the rapid clearance of new aircraft configurations. Physics-based M&S tools utilizing FSI capabilities are being evaluated to verify the ability to model and augment flight test. The overall objective of the work presented herein is to build a physics-based aeroelastic model of the AIT boom system to provide an M&S capability for evaluating future icing array designs. An accurate structural model is a prerequisite for performing high-fidelity physics-based simulations. In order to build an accurate structural model, sufficient data must be obtained describing the real system.

This work reports the GVT results used to validate a simplified FE structural model of the AIT boom system. Twenty-four configurations of the AIT boom were analyzed through a two-phase GVT. The first phase was performed with the AIT boom system detached from the aircraft. This configuration is unconstrained (free) in translation and rotation. Therefore, the free-free configuration vibration tests are denoted as the free-free GVT throughout. The second phase was performed with the AIT boom system attached to the aircraft (on-aircraft configuration). Each GVT phase was conducted with and without an array mass substitute (AMS) attached. Data collected from the GVT includes: modal frequencies, damping values, and mode shapes. Steady-state inviscid simulations were performed to assess the forces on the AIT boom system with two different array designs. An assessment of the ruddervator angle of attack, α_R on the forces encountered by each array design is presented in detail.

*773rd Test Squadron, Hypersonics Combined Test Force, AIAA member
†812th Test Support Squadron, Engineering Testing Technologies, AIAA non-member
‡773rd Test Squadron, Structures Branch, AIAA member
§812th Test Support Squadron, Engineering Testing Technologies, AIAA non-member

Motivation & Goals

The overall test objectives of the GVT were to measure the vibration characteristics of the AIT boom system for implementation into a structural model to be used for aero-structure simulation and to determine the structural vibration mode shapes, associated frequencies, and damping values of the AIT boom system with it both detached and attached to an aerial refueling representative KC-135R aircraft. The objective of the FE modeling effort is to increase confidence in M&S tools, quantify physical characteristics, and reduce overall program cost.

Validation and verification (V&V) of M&S tools is required for all pertinent tests used to compliment test and evaluation (T&E) needs. A build-up approach of M&S capabilities requires V&V with results from a previous system to be performed prior to future evaluations. It also serves to quantify the validity and build confidence in the simulated environment. Therefore, the results from the FE model are directly compared to the GVT results for validation prior to FSI simulations. Afterward, FSI simulations will be used to quantify the behavior of the AIT boom system in conditions characteristic of flight test. Once validated against flight test data, the FSI model can be used to study new array design concepts and provide array stability information prior to wind-tunnel and flight tests. The FSI model is expected to provide a measurable improvement to the design and testing of the AIT boom system. The advantage of FSI computational modeling, over computational fluid dynamics (CFD) or FE modeling and simulation alone, is the ability to better predict interactions between aerodynamic forces and structural dynamics.

II. GVT Description & Setup

Ground vibration tests are designed to determine the dynamic characteristics of an object by exciting its structure, usually with electrodynamic shakers, then recording the response with accelerometers. The response data and the input excitation are analyzed by a modal analysis tool to calculate mode shapes, frequencies, and damping values associated with the test structure. The GVT performed on the AIT boom system is described through a discussion of the setup, test article, suspension system, shaker system, accelerometer placement, system configurations, and excitation procedures.

II.A. Setup

The GVTs were performed on the AIT boom system in two phases. Phase I was a free-free GVT on the AIT boom system and phase II was a GVT on the AIT boom system while attached to a KC-135R. Phase I consisted of 14 unique configurations and phase II consisted of 10 unique configurations. Test configurations varied by shaker locations, whether or not the boom was extended, whether or not the AMS was attached, and whether or not the internal water tubes were installed. Three of the test configurations were used to validate the FE model of the AIT boom system. In all of the configurations, the boom system is entirely or partially supported with a bungee isolation suspension system.ex

II.A.1. Test Item Description

The operational AIT system provides a capability for representing natural rain and ice accumulation for conducting flight test in adverse weather conditions. The AIT boom system used in the GVT was a modified high speed aerial refueling tanker boom for the KC-135R aircraft with the AMS and gimbal with dampers attached. The AMS was used in place of the actual icing array due to parallel design testing being performed at Arnold Engineering Development Center. The AIT AMS was designed to retain comparable mass and inertial properties of the icing array. The AIT boom system is shown in Fig. 1 and the AMS includes the gimbal and dampers as shown in Fig. 1(a). An aerial refueling representative KC-135R aircraft was used during the on aircraft phases of the GVT. GVT configurations utilizing the icing boom without internal tubes were also considered. The icing boom without internal tubes system was defined as the high speed boom with all aerial refueling configuration parts removed and icing boom parts installed. Icing boom parts that were excluded from this definition were the gimbal, dampers, internal water tubes, internal bleed air tubes, and the AMS. From this point forward, the internal tubes will be referred to as water tubes.

II.A.2. AIT Boom Suspension System

The suspension system was located directly above the critical points of the AIT boom system configuration and allowed movement in six degrees of freedom. A photograph of a bungee attachment is shown in Fig. 1(b). Twelve to 15 loops of 0.5 inch diameter bungee cord was deemed sufficient to safely suspend an item weighing approximately 2000 lbs and to provide adequate response characteristics for testing. It was observed that longer lengths of bungee provided better response characteristics. However, the bungee length used should be carefully considered to avoid placing the system under test in an unsafe situation during the suspension process. Prior to testing, the approximate center of gravity of the test article was located to assist in balancing the suspended structure.

The bungee termination method used during test was sufficient to prevent bungee slippage for GVT purposes. The termination method consists of looping both ends of a 0.5 inch diameter bungee cord through a metal plate with 0.5 inch diameter holes. An additional wire rope clamp was used to tie the free lengths of bungee together should the loops through the metal plate slip.

At the beginning of testing (phase I) a bungee cord was used to secure the ruddervators to lessen freeplay effects. A cord was wrapped around the ruddervators then tied between them. However, evidence of freeplay remained due to difficulties associated with adequate tension. During phase II, a more robust solution using wood shims to secure the ruddervators and lessen freeplay was employed.

(a) Array Mass Substitute (AMS) (b) Bungee Attachment (c) Shaker Setup

Figure 1. Photographs illustrating the GVT setup.

II.A.3. Shaker Setup

Once the AIT boom system was placed on the bungee isolation suspension system, the shaker was placed near the shaker attachment point. The shaker was clamped to the top of an aircraft jack stand. In order to get the shaker to the necessary height, the aircraft jack stand was either raised or the jack stand and shaker were placed atop a shaker stand. Shaker stands were used to minimize stand vibration and chatter while raising the shaker to the necessary height. A picture of a configuration shaker setup can be seen in Fig. 1(c). In order to better excite and tune modes of interest, a mobile shaker was used. The maximum force of the shaker was 50 lbf, but the random excitations were performed at 15 lbf while the focused excitations were performed at 3-10 lbf. For this GVT, exciting the boom near its center of gravity generated adequate responses for measuring the structural modes of interest.

Wood shims were used between the shaker stands and the floor to ensure a stable stand configuration prior to test. The jack stand that was used during the GVT had significant freeplay. Therefore, turnbuckles were used to prevent the table on the jack stand from moving and cargo straps were used to secure it to

the shaker stands. The shaker was secured to the jack stand table with pieces of steel and c-clamps. To minimize the vibration translated from the shaker to the jack stand, a piece of foam was placed under the shaker to absorb vibration.

II.A.4. Accelerometer Setup

The dynamic response of the boom was measured with 24 accelerometers for the phase I configuration and 29 accelerometers for the phase II configuration. The accelerometers were placed along the boom, extension, and ruddervators to properly capture the lateral, vertical, and rotation of the boom. On the AMS, accelerometers were placed to capture lateral, vertical, rotation, and pitch motion. Roving accelerometers can be used to tune modes at higher resolution, but were not used in this study. The GVT representations of the AIT boom systems are illustrated in Fig. 2 where each node denotes an accelerometer location.

All accelerometers were mounted to a surface so that they were in plane with the AIT boom system coordinate system designated for the test. When a surface was shaped such that the accelerometer would not be in-plane with the test coordinate system when mounted directly to the surface, a small conforming balsa wood mounting block was cut so that the accelerometer would maintain proper test orientation. Balsa wood mounting blocks were used to mount accelerometers to the ruddervators and the bulkhead at the front of the boom.

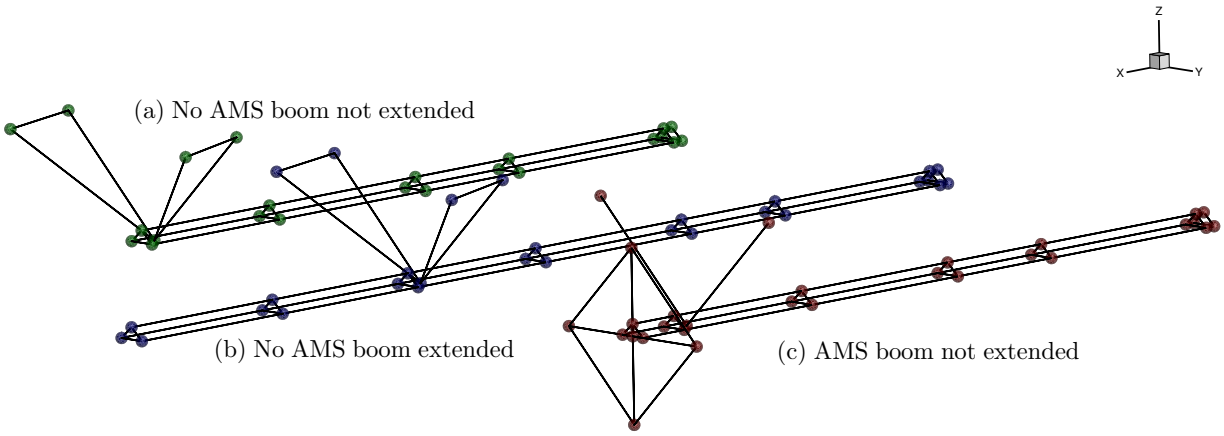

Figure 2. GVT representations of three AIT boom system configurations: (a) No AMS boom not extended, (b) No AMS boom extended, and (c) AMS boom not extended. The spherical markers correspond to accelerometer locations.

II.B. GVT Execution Procedures

The boom system was excited in the lateral and vertical directions. Random excitation was used to generate the basic structural frequency response function (FRF) to determine the vibration modes of interest up to 30 Hz. Once a mode of interest was identified through the random excitation method a sine dwell excitation was used to determine the modal frequencies with increased precision. Only the 1st lateral and vertical mode shapes and frequencies, which are below 17 Hz, are used for validation herein. The software used in this GVT includes OROS® NVGate^{TM}for data acquisition and OROS® Modal^{TM}for mode frequency and shape verification.

During the AIT boom system free-free and on-aircraft GVTs, the rigid body pitch, roll, yaw, and plunge modes were measured prior to acquiring structural modal data. These modes were well below the first structural modal frequency of the AIT boom system structure. The rigid body modes were excited manually by pushing on the boom in the appropriate direction to get the desired rigid body movement. The accelerometer response data from the rigid body modes were scrutinized to verify that all channels were working properly and oriented correctly prior to continuing each test configuration. The displacements encountered when determining the rigid body modes of the system were much larger than the displacements observed when exciting the system with a shaker, even at resonant frequency.

The structure was excited by the shaker with the continuous random excitation method. Data was captured as time histories over an adequate amount of time. Then the FRFs were plotted in the post-

processing software and adjustments in shaker location or force levels were made if deemed necessary from visual inspection. After all the data was gathered and examined, selected modes were fined-tuned. Sine dwell testing was performed on the structural modes of interest. The test director determined the final shaker configurations to best excite the various modes determined from the previous random excitation test point data. Special care was given to tailor the shaker forces to best excite the mode of interest without over-driving any component of the structure. Each mode was excited at its frequency then the excitation was terminated to allow the response to decay. Damping measurements were made indirectly for each mode excited using the logarithmic decrement method on the decay portion of the recorded response.

GVT Configurations

During the GVT numerous AIT boom system configurations were evaluated with and without the boom extended, with and without the AMS attached, and with and without the water tubes installed. The test configurations were excited vertically, laterally, or vertically on the AMS. Phase I of the AIT GVT was performed with the AIT boom system fully suspended on the bungee isolation suspension system which was hung from an I-beam. The configurations for phase I are given in Table 1. Phase II of the AIT GVT was performed with the AIT boom system attached to a KC-135R and are given in Table 2.

Table 1. Phase I test configurations for the AIT boom system in the free-free configuration.

Config.	Boom Extended	AMS Attached	Internal Tubes Installed	Excitation Type
1				Vertically
2				Laterally
3	✓			Vertically
4	✓			Laterally
5			✓	Vertically
6			✓	Laterally
7	✓		✓	Vertically
8	✓		✓	Laterally
9		✓	✓	Vertically
10		✓	✓	Laterally
11		✓	✓	AMS Vertically
12	✓	✓	✓	Vertically
13	✓	✓	✓	Laterally
14	✓	✓	✓	AMS Vertically

Table 2. Phase II test configurations with the AIT boom system attached to the KC-135R aircraft.

Config.	Boom Extended	AMS Attached	Internal Tubes Installed	Excitation Type
15			✓	Vertically
16			✓	Laterally
17	✓		✓	Vertically
18	✓		✓	Laterally
19		✓	✓	Vertically
20		✓	✓	Laterally
21		✓	✓	AMS Vertically
22	✓	✓	✓	Vertically
23	✓	✓	✓	Laterally
24	✓	✓	✓	AMS Vertically

III. Discussion of GVT Results

Post-test data analysis was performed on all 103 tuned modes. To determine the proper modal frequencies of modes, Lissajous plots were used to tune the modal frequencies. For each mode the accelerometers with the greatest amplitude responses that corresponded with the mode shape were selected for damping calculations. The average of multiple calculated damping values were reported for each mode. In some cases a damping value was calculated even though it was apparent that there were two closely coupled modes present in the decay time history. In these cases, the damping value should be viewed as an estimated value. The GVT results are reported in greater detail by Besson.[1]

III.A. Phase I: Free-Free Configurations

In configuration 5 the AIT boom system is freely suspended on bungees while being excited vertically with the water tubes installed (not extended) without the AMS attached. The 1st mode was observed at 10.25 Hz and exhibited 2nd bending in the boom with ruddervator motion and an average damping value of 2.22%. The 2nd mode was observed at 16.95 Hz revealing a 2nd bending mode in the boom with ruddervator motion boom motion and an average damping value of 4.77% and its corresponding mode shape given in Fig. 3(a,b). The 3rd mode was observed at 46.75 Hz was clearly the 3rd bending in the boom with trailing edge ruddervator motion and had a measured average damping value of 4.09%.

Configuration 6 is similar to that of configuration 5, but the boom is being excited laterally. The 1st mode observed at 8.9 Hz was the typical 2nd lateral bending in the boom with ruddervator motion and had a measured average damping value of 2.24% and its corresponding mode shape is given in Fig. 3(c,d). The 2nd mode was observed at 11.1 Hz exhibited 2nd bending with lateral rigid body motion and ruddervator motion. The 3rd mode observed at 12.08 Hz is best described by the 2nd lateral bending in the boom with rotation and ruddervator motion. The 4th mode was tuned at 13.37 Hz yielded 2nd lateral bending of the boom with rotation and a measured average damping value of 3.58%. The 5th mode observed at 34.35 Hz was the 3rd lateral bending in the boom with ruddervator motion and a measured average damping value of 7.88%.

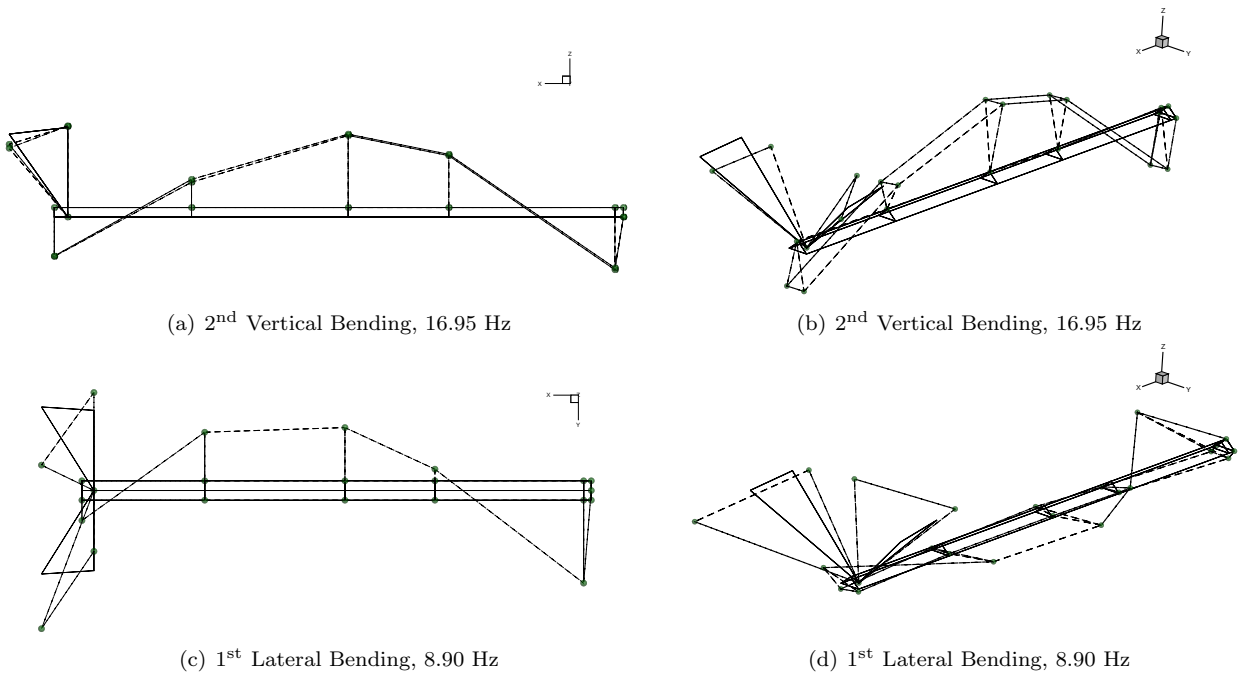

(a) 2nd Vertical Bending, 16.95 Hz

(b) 2nd Vertical Bending, 16.95 Hz

(c) 1st Lateral Bending, 8.90 Hz

(d) 1st Lateral Bending, 8.90 Hz

Figure 3. Primary bending mode shape for configurations 5 & 6: free-free, no AMS, vertical and lateral excitation. Solid lines show original geometry while dashed lines show mode shapes.

In configuration 7 the AIT boom system is freely suspended on bungees, boom extended, without the AMS installed while being excited vertically. The 1st mode observed at 5.9 Hz was 2nd lateral bending in the boom and extension with an average damping value of 2.32% and its mode shape is visualized in Fig. 4(a,b).

The 2nd mode observed at 10.43 Hz was 2nd bending in the boom and extension with ruddervator motion. The 3rd mode observed at 16.5 Hz was 3rd bending of the boom and extension with an average damping value of 3.01%. The 4th mode observed at 32.28 Hz was 4th bending in the boom and extension with an average damping value of 2.38%.

Configuration 8 differs from configuration 7 only in the fact that it utilized lateral excitation. The 1st mode observed at 4.57 Hz was 2nd lateral bending in the boom and extension with an average damping value of 1.72% and its mode shape is visualized in Fig. 4(c,d). The 2nd mode observed at 9.5 Hz was 3rd lateral bending in the boom and extension with ruddervator motion and an average damping value of 2.31%. The 3rd mode observed at 12.83 Hz was 3rd lateral bending in the boom and extension with rotation and ruddervator motion, but there was insufficient instrumentation to properly capture the mode shape. The 4th mode observed at 35.36 Hz was 4th lateral bending of the boom and extension with rotation and ruddervator motion, but it also lacked adequate instrumentation to properly capture the mode shape.

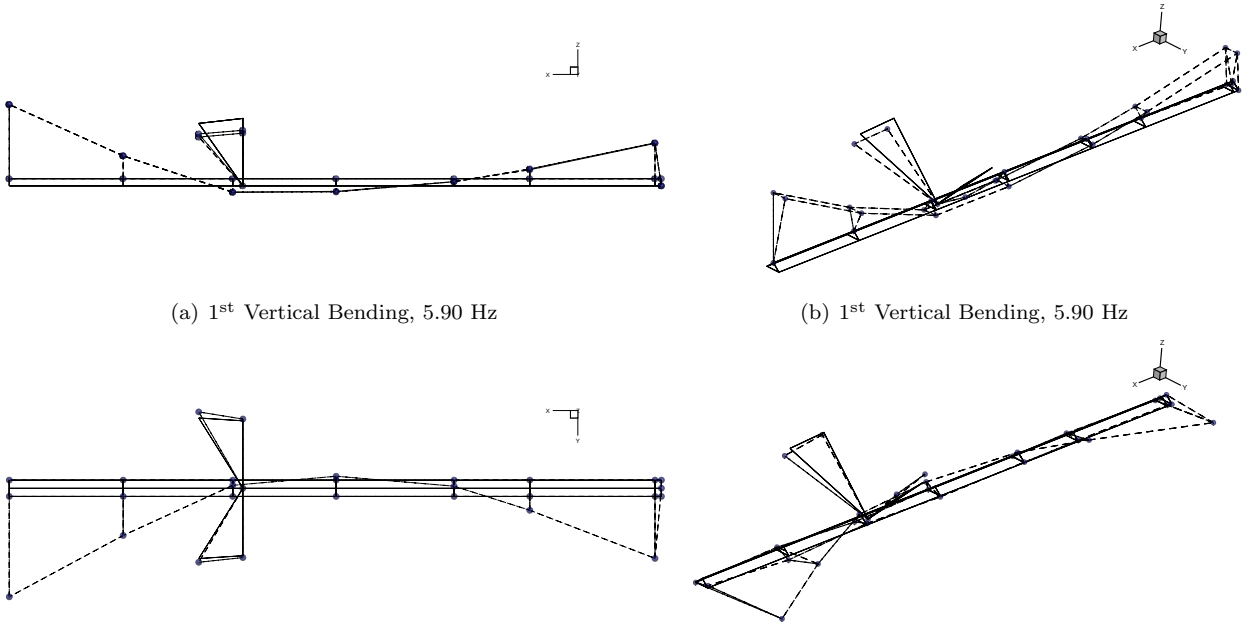

(a) 1st Vertical Bending, 5.90 Hz

(b) 1st Vertical Bending, 5.90 Hz

(c) 1st Lateral Bending, 4.57 Hz

(d) 1st Lateral Bending, 4.57 Hz

Figure 4. Primary bending mode shape for configurations 7 & 8: free-free, no AMS, vertical and lateral excitation with boom extended. Solid lines show original geometry while dashed lines show mode shapes.

III.B. Phase II: Attached to the KC-135R

In configuration 15 the AIT boom system is attached to the KC-135 aircraft without the AMS attached in the non-extended configuration while being excited vertically. The 1st mode observed at 8.99 Hz was 2nd bending of the boom with motion in the ruddervators with an average damping value of 4.40%. The 2nd mode observed at 15.95 Hz was 2nd bending in the boom without ruddervator movement with an average damping value of 4.90% and its mode shape is visualized in Fig. 5 (a,b). The 3rd mode observed at 35.00 Hz was 3rd bending in the boom with a lot of ruddervator movement with an average damping value of 7.43%.

Configuration 16 differs from configuration 15 in that the system is being excited laterally. The 1st mode observed at 4.78 Hz was a rotation mode in the boom with an average damping value of 4.37%. The 2nd mode observed at 6.91 Hz was 2nd lateral bending with rotation on the ruddervators with an average damping value of 2.06% and its mode shape is visualized in Fig. 5(c,d). The 3rd mode observed at 11.7 Hz was 2nd bending with ruddervator motion with an average damping value of 3.86%. The 4th mode observed at 21.6 Hz was 3rd lateral bending with rotation in the boom, but there may have been insufficient instrumentation to properly capture this mode.

In configuration 19 the AIT boom system is attached to the aircraft with the AMS attached to the non-extended boom that is being excited vertically. The 1st mode observed at 8.76 Hz was 2nd bending of the boom with vertical and pitch motion of the AMS and a lot of motion in the ruddervators. Post-test analysis

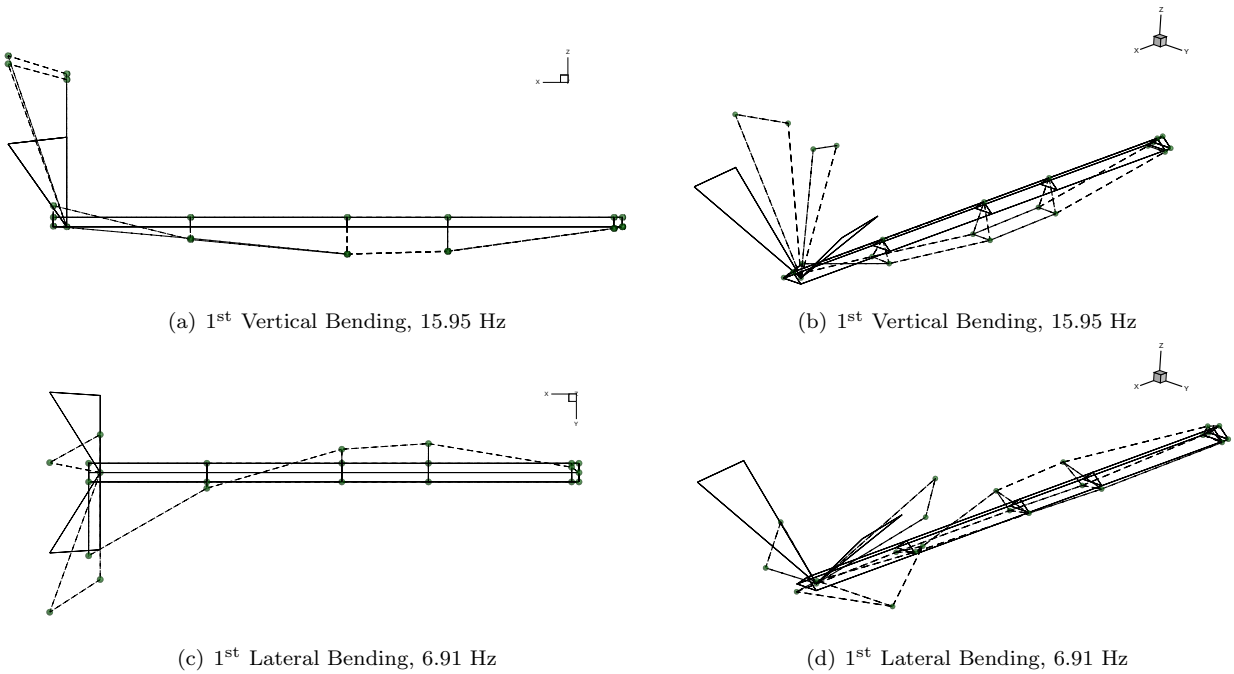

(a) 1st Vertical Bending, 15.95 Hz

(b) 1st Vertical Bending, 15.95 Hz

(c) 1st Lateral Bending, 6.91 Hz

(d) 1st Lateral Bending, 6.91 Hz

Figure 5. Primary bending mode shape for configurations 15 & 16: on-aircraft, no AMS, vertical and lateral excitation. Solid lines show original geometry while dashed lines show mode shapes.

showed that the observed frequency did not adequately excite the mode of interest. The 2nd mode observed at 15.78 Hz was 2nd bending of the boom with some vertical and pitch motion of the AMS with an average damping value of 2.32%. The 3rd mode observed at 28.68 Hz was 3rd bending of the boom with vertical and pitch motion of the AMS and ruddervator movement. Post-test analysis of the accelerometers that exhibited the largest response amplitudes on the boom-array attachment and the AMS revealed a calculated average damping value of 3.04%.

In configuration 20 the AIT boom system is attached to the aircraft with the AMS attached to the non-extended boom that is being excited laterally. The 1st mode observed at 4.75 Hz was 2nd lateral bending of the boom with lateral motion of the AMS and motion in the ruddervators with an average damping value of 10.08%. The 2nd mode observed at 8.36 Hz was a combination of 2nd lateral and 2nd vertical bending with motion in the ruddervators and lateral motion of the AMS, but post-test analysis showed that the mode of interest was not excited properly. There could be coupling between 2 modes at this frequency as the MIF plot shows a possible double peak around the observed frequency. The 3rd mode observed at 12.36 Hz was 2nd lateral bending with motion at the end of the boom and AMS with an average damping value of 3.62%. The 4th mode observed at 18.88 Hz was 3rd lateral bending with motion at the end of the boom and AMS with an average damping value of 2.89%.

IV. Finite Element Modal Model

The structural model is completely created using data from the GVT tests and general knowledge derived from the physical boom. Only general two- and three-dimensional CAD models of this system were available. These models did not include internal boom structure, but the physical boom was available for modeling purposes. The mass, mass distribution, and moments of inertia were not quantified due to budget constraints. The details given in this section demonstrate the validation procedure of a simplified FE modal model via comparison with GVT results for mode frequency and shape. The FE solver used in this work is the commercially available code known as AERO-S which is a modal and/or full FE dynamic non-linear solver utilized by the 8th Test Support Squadron M&S group and is part of the AERO Suite of Codes.[2]

IV.A. Discretization and Element Types

The model used for this investigation is a stick FE model built in AERO-S format. The boom models consist primarily of beam elements that represent both the outer structural boom and the telescoping internal tube. The outer structural boom and the inner structural telescoping boom are collocated in the model. The models of these beams are constant and are not changed between configurations. The only changes made between the models are the relative location of each beam (extended and not extended), and the boundary conditions where the structural parts are in contact and the attachment to the aircraft. The ruddervators were assumed to be rigid. Rigid beam elements and phantom shell elements were used to ensure that the boom model is conformal with the intended CFD model and give the model the appearance that it is a representative boom.

Bernoulli beam elements with six degrees of freedom per node are used to model the water tubes. Each tube was discretized with 101 elements. The material properties of the beam elements contain the varying cross-sectional areas and cross-sectional moments of inertia that represent the geometric and mass variations in the modified refueling boom. The Young's modulus E=10^7 [psi], Poisson's ratio ν=1/3, and mass density ρ=7.5×10^{-4} [snails/in^3] are identical for each beam element used. For damper elements, three-dimensional, 2-node rigid beam elements are used to enforce constant length, equal rotations of the cross sections at its two nodes, and constraints between its rotational and translational DOFs. The results presented use two different boundary conditions representing the free-free and attached phases of the GVT.

IV.B. Validation with GVT Results

IV.B.1. Modal Frequencies

The model frequencies are compared to values obtained from the GVT in Table 3. The structural finite element model (FEM) was verified both with and without the rigid beam and phantom shell elements by ensuring structural characteristics were not affected by the addition of these fictitious elements. This table presents the GVT and FEM mode frequencies and the error associated with the FEM model. Good agreement between the FEM and GVT is demonstrated for the free-free (phase I) configurations, but the frequency associated with the 1st vertical bending mode for the phase II configuration is 17.5% greater than that observed from the GVT. It is important to stay within the ±3% error military specification[3,4] for cases involving flutter where a small error in mode frequency can drastically alter the flutter boundary.[5] Owing to the geometric and material nonlinearities in the AIT boom system, this modal model does not meet that specification for all configurations, but is sufficient for simulations where the goal is not to simulate divergence or flutter-like phenomena.

Table 3. AIT Boom GVT and FE model mode frequency comparisons for the 1st vertical and 1st lateral bending modes.

Mode		Configurations 5&6 Free-Free Not Extended Water Tubes Installed No AMS	Configurations 7&8 Free-Free Extended Water Tubes Installed No AMS	Configurations 15&16 Attached Not Extended Water Tubes Installed No AMS
1st Lateral	GVT	8.90 Hz	4.57 Hz	9.20 Hz
	FEM	8.23 Hz	4.57 Hz	9.52 Hz
	Error	−7.53 %	0.00 %	+3.48 %
1st Vertical	GVT	16.95 Hz	5.90 Hz	10.19 Hz
	FEM	16.01 Hz	5.94 Hz	11.97 Hz
	Error	−5.546 %	+0.068 %	+17.50 %

American Institute of Aeronautics and Astronautics Paper 2013-(Control ID:1420821)

IV.B.2. Mode Shapes

In order to confirm that the modal vectors from the FE model are in good agreement with those measured from the GVT, a modal assurance criteria (MAC) was employed. It is defined as[6]

$$\mathrm{MAC}_{ij} = \frac{[\mathbf{u}_i^T \mathbf{e}_j]^2}{[\mathbf{u}_i^T \mathbf{u}_i][\mathbf{e}_j^T \mathbf{e}_j]} \tag{1}$$

where $\mathbf{u}_i$ is the ith mode shape vector from the FE model results, and $\mathbf{e}_i$ is the ith mode shape vector from the GVT. The MAC takes on values from zero to unity where zero represents no correspondence and unity represents a consistent correspondence in mode shape. Errors, or poor correspondence, are most commonly associated with model assumptions and modal parameter estimation techniques from the GVT.

The MAC for the first four modes of the free-free and attached configurations without the AMS are given in Fig. 6. In Fig. 6(a), the first two FE model mode shapes in the free-free configuration are relatively well correlated with the GVT yielding MAC values of 0.59 and 0.49 respectively. The third mode is also in slightly better agreement with a value of 0.54, but the fourth mode shape shows nearly zero correlation (0.03). In Fig. 6(b) the MAC for the on-aircraft configuration reveals less correlation than that obtained in the free-free configuration. However, the first vertical mode shape demonstrates a MAC similar to the free-free configuration at 0.55. The fourth mode shape of the FE model is correlated with the second mode shape of the GVT. The physical AIT boom has inherent geometric and material non-linear characteristics which creates difficulties when comparing modal (linear) responses.

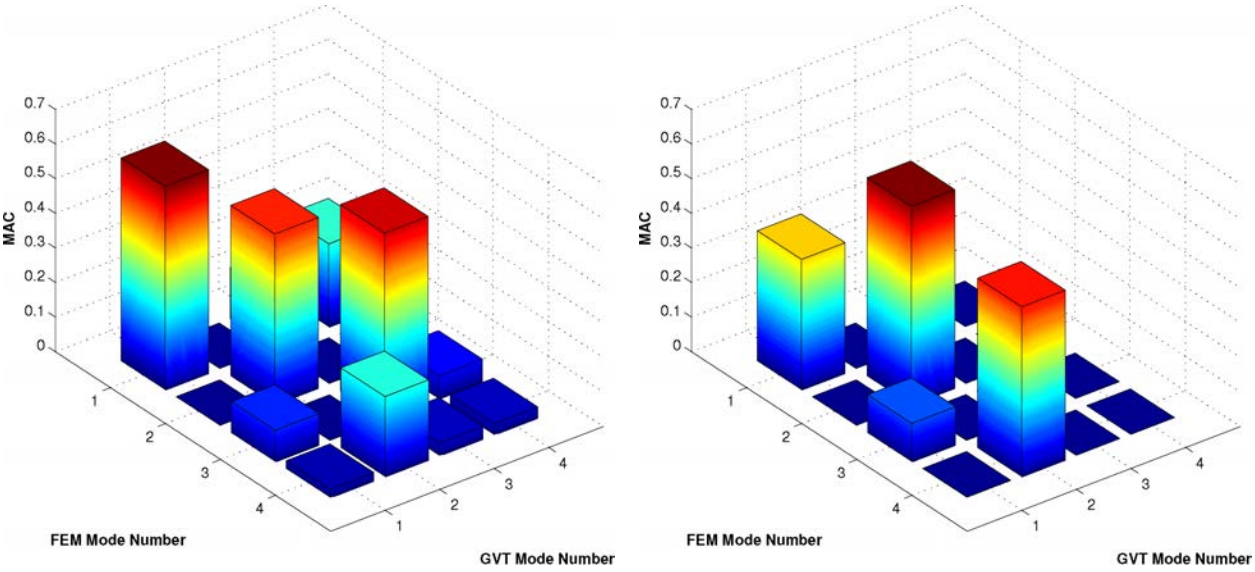

(a) Free-Free (Configs. 5&6)

(b) Attached (Configs. 15&16)

Figure 6. MAC for the first four modes, i.e., lateral and vertical 1st and 2nd bending.

V. Inviscid Aerodynamic Simulations

V.A. Fluid Solver Details

The AERO-F Suite[2] is used for the inviscid aeroelastic simulations presented in this work. The methodology for the code is largely based on the work of Farhat and coworkers[7–12] efforts towards the development of second-order accurate aeroelastic employing the arbitrary-Lagrangian-Eulerian (ALE) formulation for moving unstructured grids. This suite has been used to study aeroelastical phenonema of fighter aircraft. Specifically, the F-16[12–15] has been investigated in numerous configurations and flight conditions.

The numerical methods employed during these simulations include 2nd-order accurate spatial reconstruction utilizing a Galerkin based reconstruction of nodal gradients utilizing the Van Albada limiter[16] and the implicit three-point backward difference time integration scheme. The matrix-vector products associated

American Institute of Aeronautics and Astronautics Paper 2013-(Control ID:1420821)

with the time integration were chosen to be computed exactly. The number of Newton iterations is limited to unity while the maximum number of GMRES[17] iterations, as well as Krylov vectors used in the linear equation solver, was chosen to be 256. The restricted additive Schwarz algorithm[18] (RAS) based pre-conditioner was used to assist the linear equation solver in reaching a relative residual tolerance of 10^{-3}. For these steady-state computations, solution convergence was determined when the global relative residual requirement of $\|r\|/\|r_0\|=10^{-6}$ was achieved. However, forces on the AIT boom system were also monitored for convergence as well.

The ruddervators can be moved about their axes of rotation to a desired angle of attack α_R in order to monitor the influence ruddervator, the boom, and the array separately. The mesh motion scheme used for mesh movement utilizes a single-level mesh motion algorithm characterized by the robustness of a ball vertex spring analogy and leverages the ALE formulation of AERO-F. The number of increments used to deform the mesh in the vicinity of the ruddervators to a specified α_R is 1. The linear system associated with the mesh motion is solved using the conjugate-gradient[19] iterative solver in conjunction with a Jacobi pre-conditioner since matrices of this type are diagonally dominant. The maximum number of Krylov vectors and iterations were both set to sixty-four. The tolerance for the relative residual associated with the mesh-motion linear system was 10^{-3}.

V.B. Fluid Domain Setup

The fluid mesh used for the inviscid simulations of the flow around the AIT with boom and array is an unstructured grid generated with ANSYS® ICEM CFD™ containing 5.8 million grid points with 29.3 million tetrahedron volume elements. This particular mesh is homogeneous lacking a fine prism layer near the aircraft, boom, or array boundaries since the no-slip condition is not enforced. The surface mesh of the full aircraft configuration is given in Fig. 7(a) and the surface mesh of the icing assembly is given in Fig. 7(b). A cut plane of the tetrahedral volume mesh for the full aircraft is given in Fig. 8(a) and the icing assembly area is given in Fig. 8(b). In Fig. 8(a) it is evident that the majority of the grid resolution was focused near the surface of the aircraft. More specifically, the grid density in the vicinity of the array is much finer than any other part of the grid as seen in Fig. 8(b). Two different Euler fluid grids were used in the study of the ruddervator angle of attack, α_R, on the forces on the boom and ruddervators as well as the array. One grid was constructed with the ruddervators initially at an angle of attack of α_R=0.42° while the second was constructed with the ruddervators at an angle of attack of α_R=9.42°.

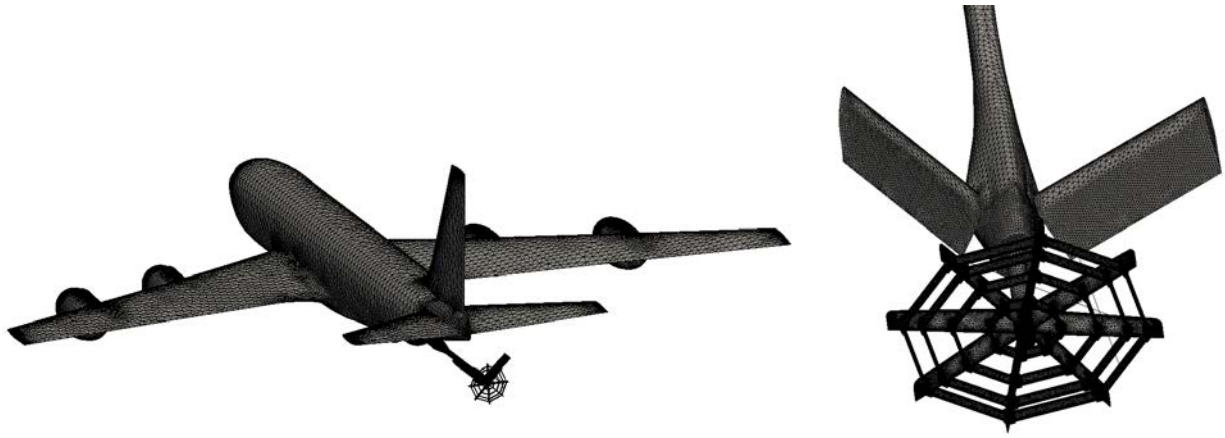

(a) Full Aircraft (b) Icing Assembly Detailed View

Figure 7. Inviscid fluid surface triangulation for (a) the full aircraft configuration and (b) the octagon icing array area.

The fluid mesh used for the inviscid simulations of the flow around the AIT with boom and the round array design is an unstructured grid containing approximately 4.0 million grid points corresponding to 23.6 million tetrahedron volume elements. As with the octagon array, this particular mesh contains only tetrahedral elements and does not contain a fine prism layer near the aircraft, boom, or array wetted surface. The surface mesh of the full aircraft configuration is given in Fig. 9(a) and the surface mesh of the round icing array is given in Fig. 9(b). A cut plane of the tetrahedral volume mesh for the full aircraft is given in Fig. 10(a) and the icing assembly area is given in Fig. 10(b). In Fig. 10(a) it is evident that the majority of

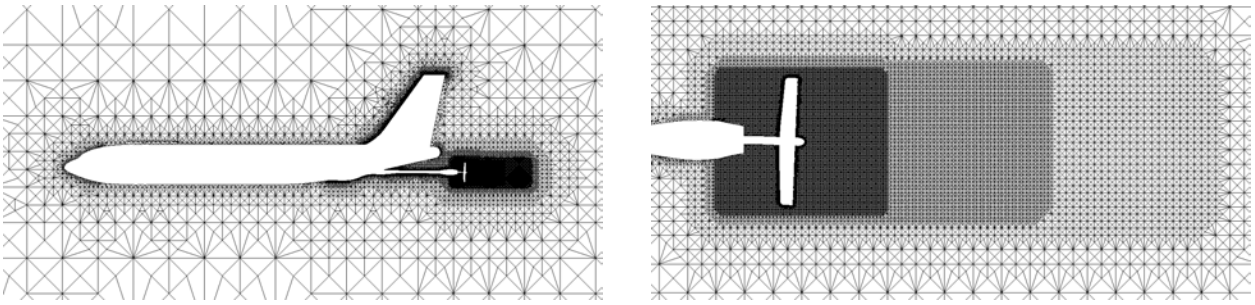

(a) Full Aircraft (b) Icing Assembly Detailed View

Figure 8. Inviscid fluid tetrahedral volume mesh cut plane for (a) the full aircraft configuration and (b) the octagon icing array area.

the grid resolution was focused in the near-field region of the array. Only one grid was used in this study and was constructed with the ruddervators initially at α_R=5.42°.

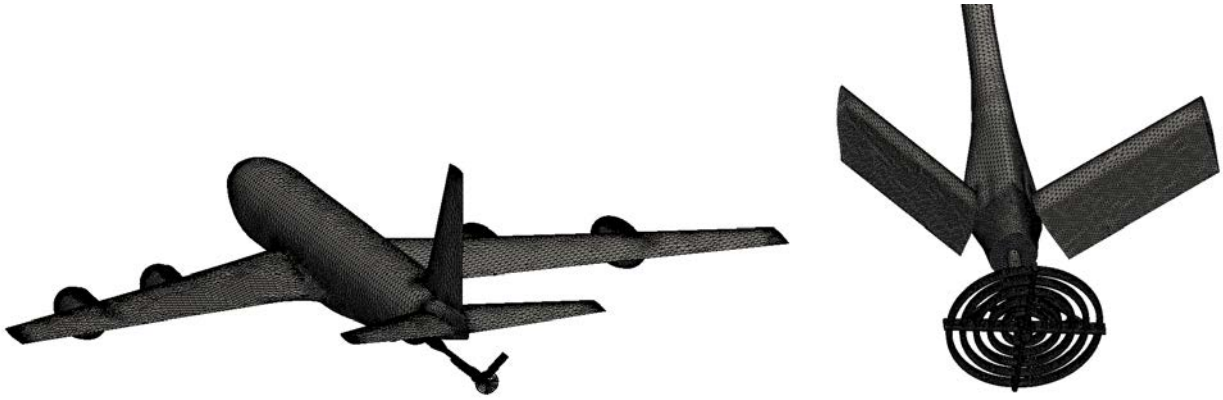

(a) Full Aircraft (b) Icing Assembly Detailed View

Figure 9. Inviscid fluid surface triangulation for (a) the full aircraft configuration and (b) the round icing array area.

V.C. Flight Conditions

All of the simulations in this work were performed at a single flight condition. The physical description of the flight condition is given by a Mach number of M_∞=0.398, an angle of attack of α=0.42°, a sideslip angle of β=0.0°, and altitude of 10,000 feet having an ambient pressure of p_∞=10.10 psi and a density of ρ_∞=8.46×10^{-8} snails/in^3.

V.D. Inviscid Steady Simulation Results

Steady simulations are performed using implicit time integration with an initial CFL number of 10. The maximum CFL number is limited to 2000 to mitigate stability issues. The residual as well as the forces are monitored to ensure convergence for these steady state simulations. A typical convergence history for the relative residual $\|r\|/\|r_0\|$ is given in Fig. 11(a) and for the total forces in Fig. 11(b). Figure 11(a) demonstrates that the relative residual reaches a converged solution criteria of 10^{-6} in slightly less than 250 iterations for the α_R=0.42° case. Figure 11(b) demonstrates that the forces on the array converge rapidly as well. The convergence history in these two plots is typical of the steady-state simulations presented herein.

Figure 12 presents the force in the stream-wise (x) and gravitational (z) directions respectively versus the ruddervator angle of attack, α_R. The x-component of the force experienced by the individual components remains relatively constant for several α_R values as indicated by Fig. 12(a). In Fig. 12(b) the $+z$ (opposite of gravity) component of force is given for the separate elements of the boom and array assembly as well as the total force generated versus α_R. The total weight of the boom-array combination structural model

American Institute of Aeronautics and Astronautics Paper 2013-(Control ID:1420821)

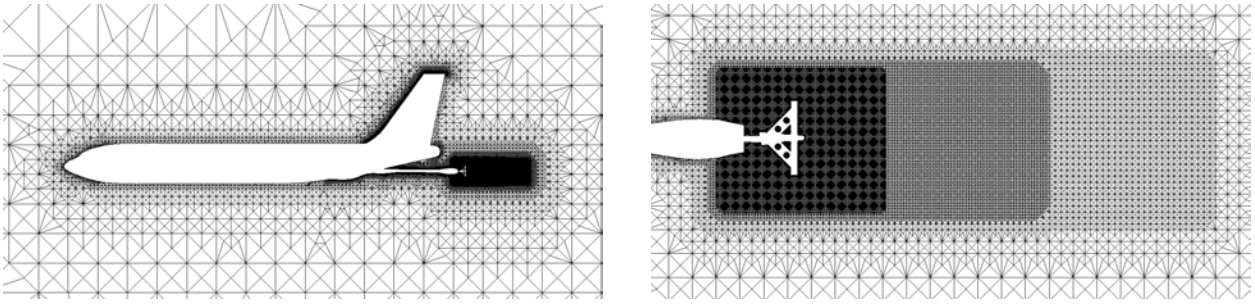

(a) Full Aircraft (b) Icing Assembly Detailed View

Figure 10. Inviscid fluid tetrahedral volume mesh (4.0 million grid points, 23.6 million tetrahedrons) cut plane for (a) the full aircraft configuration and (b) the round icing a rray area.

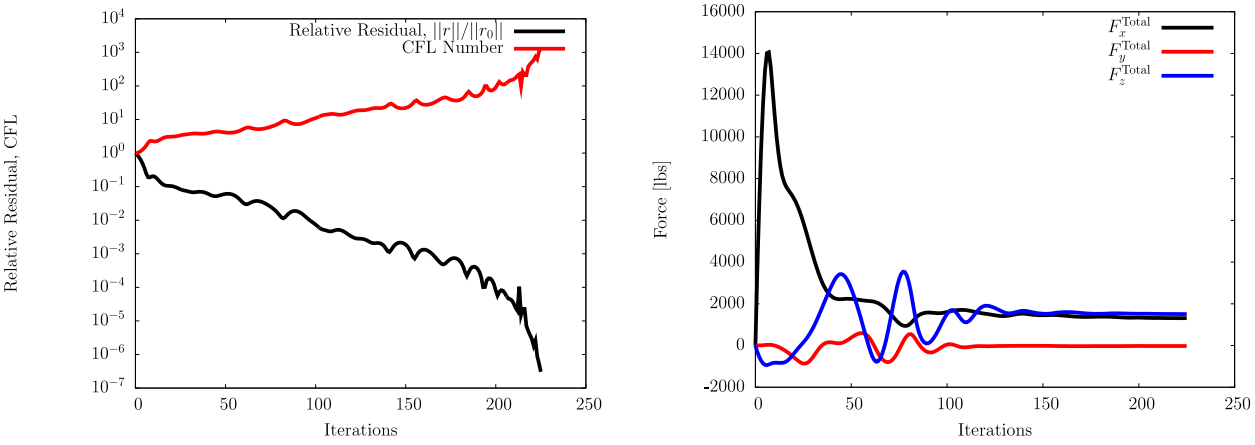

(a) $\|r\|/\|r_0\|$, CFL (b) F_x, F_y, and F_z

Figure 11. Convergence history for the relative residual, $\|r\|/\|r_0\|$, and for the total forces F_x, F_y, and F_z on the boom for α_R=0.42°.

American Institute of Aeronautics and Astronautics Paper 2013-(Control ID:1420821)

is approximately 1477 lbs. When the aircraft is at an angle of attack of 0.42° and the ruddervator is at an angle of attack of 4.6°, the total z force generated by the icing assembly is equal to the structural model weight. When the ruddervators are at zero angle of attack, the amount of lift generated by the array is in excess of 400 lbs while the ruddervators generate a small amount of lift. As the ruddervator angle of attack is increased, the total force generated by the icing assembly increases, but the lift generated by the array itself is decreased. Furthermore, as α_R is increased up to 10.42°, the total amount of lift steadily increases, but at α_R>9.42°, the amount of lift generated by the array is negative.

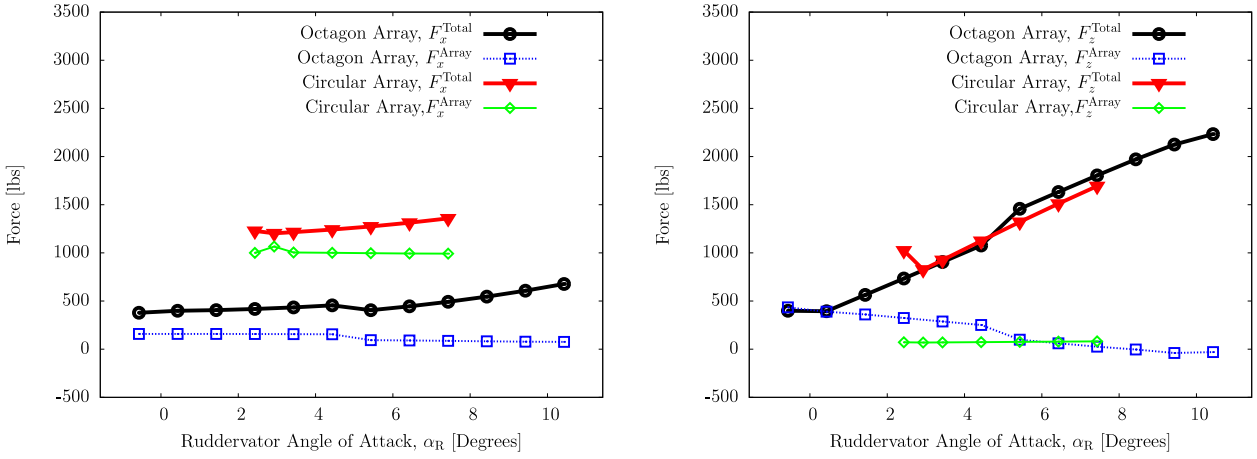

(a) F_x (b) F_z

Figure 12. Summary of x and z components of forces on the AIT octagon- and circular-shaped arrays and on the total AIT systems plotted against ruddervator angle of attack, α_R. The full AIT aircraft was at M_∞=0.398, α=0.42°, and at an altitude of 10,000 feet.

The amount of drag on round array configuration is considerable and exceeds 1000 lbs. for all α_R investigated as seen in Fig. 12(a). The majority of the drag is due to the array itself. The round array does not generate any appreciable amount of lift for any of the α_R investigated, but the AIT system is still capable of generating lift values in excess of its weight. The pitching moment about the boom mount point is given in Fig. 13 for the α_R investigated. Here the trend is identical to the trend for the lift force previously discussed. The contribution of the array on the overall pitching moment is minimal.

The considerable difference between the octagon array and the round array were the effects of the ruddervator angle of attack on the lift force on the array itself. In Fig. 12(b) we can see that the overall lift predicted for the round array is similar to that of the octagon array for the α_R investigated. However, what is promising is that the round array holds a constant lift value for the entire range of α_R which was not the case with the octagon Array. As a result, the moment about the damper will remain nearly unchanged for a range of α_R under aerodynamic loading which could be a promising result for minimizing instabilities encountered with the octagon-shaped array.

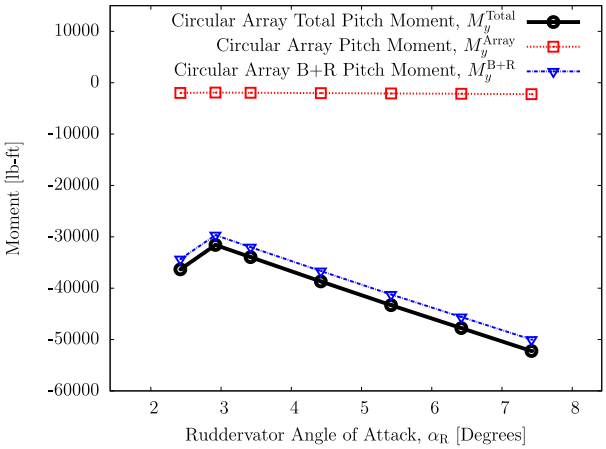

Figure 13. The pitching moment, M_y on the AIT boom, ruddervator, and round array for different ruddervator angles of attack. The full AIT aircraft was at M_∞=0.398, α=0.42°, and at an altitude of 10,000 feet.

The pressure distribution on the surface of the octagon-shaped array icing assembly is given in Fig. 14 for the undeformed fluid grids with α_R=9.42° and 0.42°. The surface contours reveal that for the α_R=9.42° case, flow over the ruddervators is likely higher speed due to the presence of the low pressure cool-colored contour near the leading edge of the upper surface. Also visible are the high pressures on the leading edge of the array airfoils indicated by warmer colors illustrating that the stagnation point is on the upper surface of the array airfoils above the boom centerline generating a net downward force. The surface contours for the α_R=0.42° case hint at lower speed flow over the ruddervators, but higher speed flow

American Institute of Aeronautics and Astronautics Paper 2013-(Control ID:1420821)
Pending Distribution A: "Approved for public release; distribution is unlimited." - AFFTC-PA-XXXX

over the upper surface of the array airfoils located above the boom centerline. This high speed flow over the array airfoils is the most likely reason that the array generates a significant amount of lift for the α_R=0.42° case as seen in Fig. 12(b). The inviscid simulations performed in this study indicate that the flow through the array is primarily the flow coming off the KC-135R wing root. By assuming that the flow is inviscid, in addition to using a coarse grid in the vicinity of the AIT wings, small and medium scale structures in the wing wakes could not be resolved.

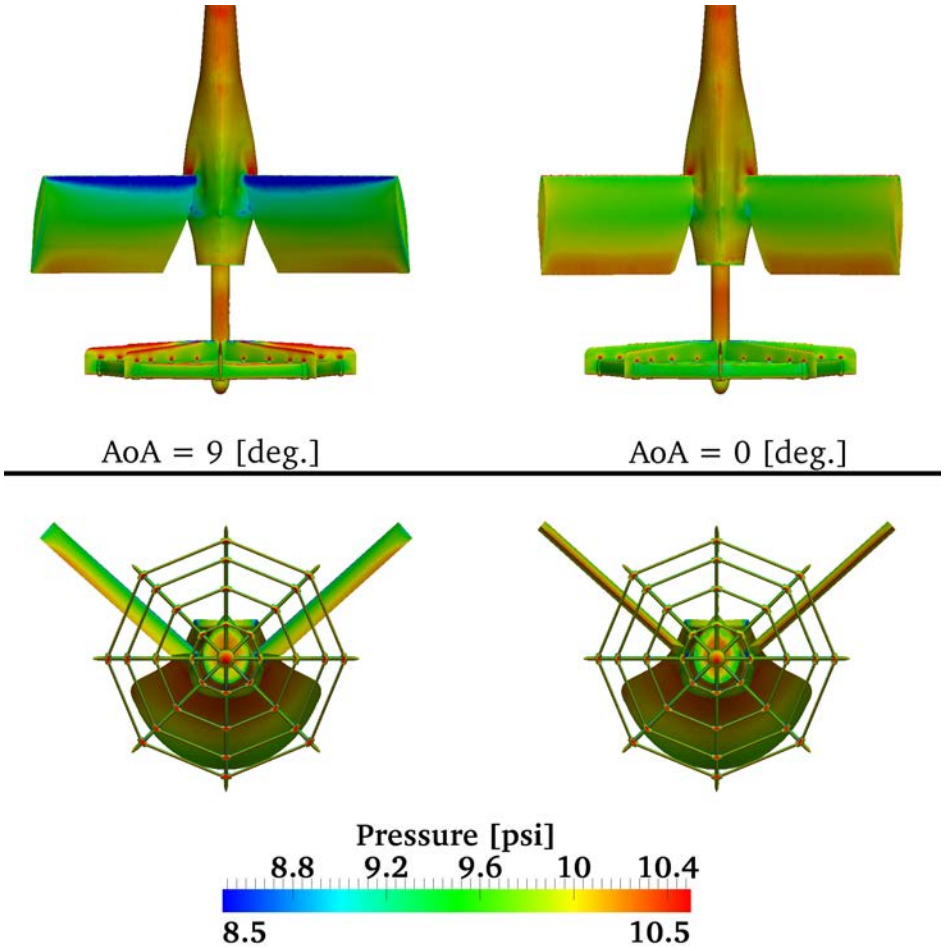

Figure 14. Pressure contours on the surface of the AIT icing assembly for α_R=9.42° and 0.42°.

Figure 15 displays x-velocity contours in knots and pressure contours in psi for the center cut-plane at α_R=5.42° and M_∞=0.398, α=0.42° and an altitude of 10,000 feet. In Fig. 15(a) the velocity contours show recirculation regions predicted by the steady inviscid simulation performed where the colors are cooler. Streamlines were seeded by using a distribution of 50 random points within a distance of 26 inches from the array center to determine the origin of the flow through the array. Figure 16(a) shows that the origin of the streamlines passing through the array originate from the bottom of the aircraft and not from the aircraft wings. A detailed view of those streamlines is given in Fig. 16(b) with an emphasis on the recirculation region near the boom-tube interface as depicted in the u_x contours in Fig. 15(a).

Several simulations have been performed under a single aircraft flight condition while the ruddervators on the boom were moved through several angles of attack. Figure 17 displays the centerline cut-plane for the stream-wise velocity, u_x for the entire aircraft (a) and in the region near the array (b) for both the octagon array and the round array design. The warmer colors represent to high speed flow with a maximum of approximately 300 knots and the cooler colors represent low speed flow with a minimum of approximately -100 knots in the recirculation regions. This cut plane shows a major difference in blockage from the two arrays. The round design reduces the downstream flow by approximately 100 knots for several diameters downstream and the octagon array only reduces the near field downstream.

The blockage of the flow seen in Fig. 17 corroborates the large difference in drag for the two array designs.

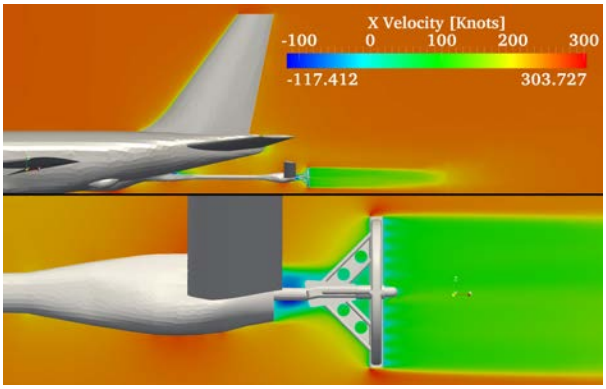

(a) u_x Contours

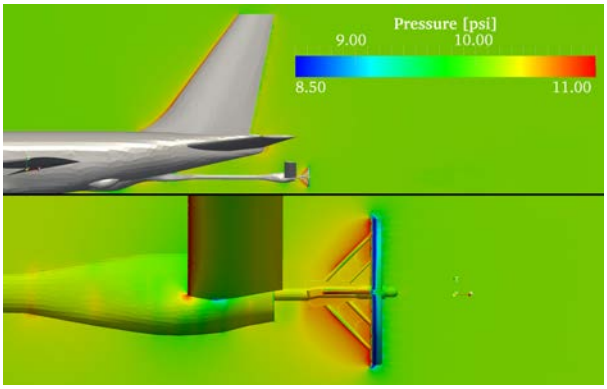

(b) Pressure Contours

Figure 15. Pressure and velocity contours in the center cut-plane of the round array design with α_R=5.42°. The full AIT aircraft is at flight conditions of M_∞=0.398, α=0.42°, and at an altitude of 10,000 feet.

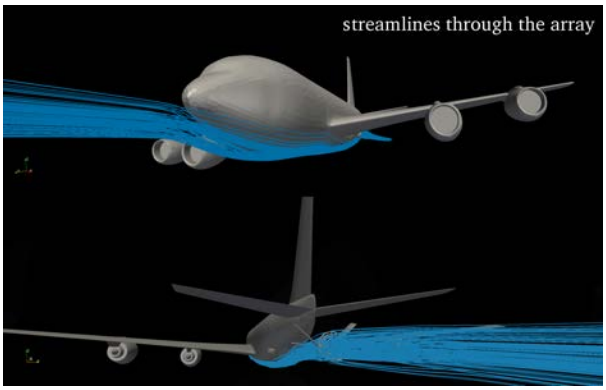

(a) Full Aircraft Views

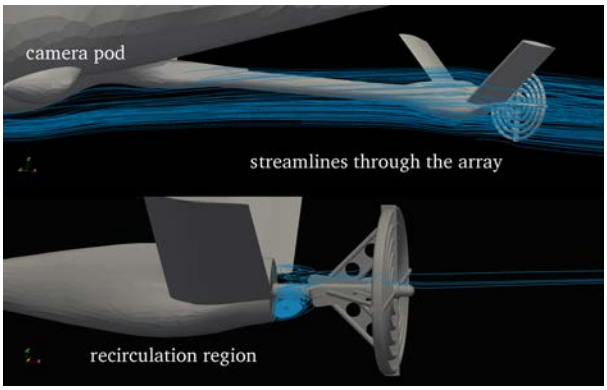

(b) Detailed Views

Figure 16. Streamlines through the round array design with α_R=5.42°. The full AIT aircraft is at flight conditions of M_∞=0.398, α=0.42°, and at an altitude of 10,000 feet.

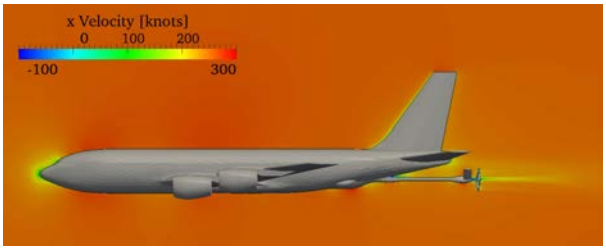

(a) Full Aircraft View (octagon)

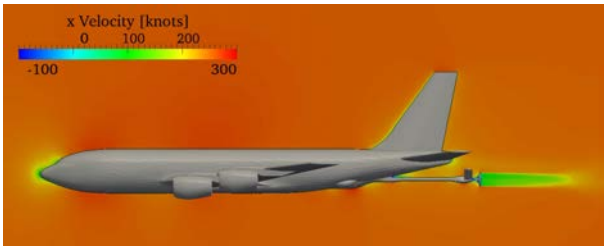

(b) Full Aircraft View (round)

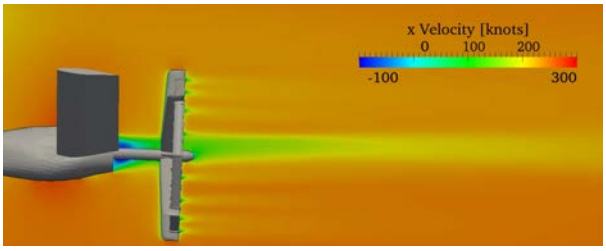

(c) Detailed View (octagon)

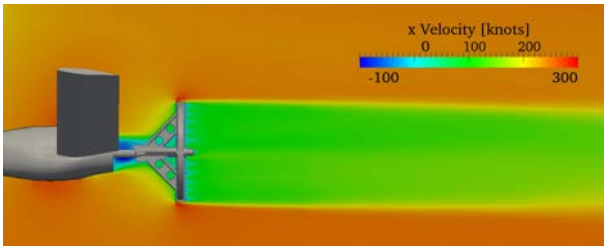

(d) Detailed View (round)

Figure 17. Comparisons of the u_x center cut-plane velocity for the AIT with the octagon and round arrays. The full AIT aircraft was at M_∞=0.398, α=0.42°, and at an altitude of 10,000 feet for both cases.

American Institute of Aeronautics and Astronautics Paper 2013-(Control ID:1420821)

Figure 12(a) shows that the drag for the octagon array and the round design are relatively constant for the ruddervator α_R tested, but the magnitude is much different, i.e., the total drag on the icing assembly is approximately tripled when going from the octagon array to the round design.

VI. Conclusions

The focus of this work was to develop an a modal structural model for the high-speed AIT boom for use with current M&S tools used to evaluate future icing array design feasibility. The work presented herein highlights a collaborative effort of the two test squadrons where the structures branch of the 773 test squadron performed a GVT of the AIT boom system and the testing techniques flight M&S group built a modal FEM model and inviscid grid for performing fluid-structure interaction simulations at representative flight conditions.

There were many lessons learned from the GVT as well as the modeling process. During the GVT process it was apparent that the boom contained many nonlinearities that were not sufficiently mitigated by the shaker force input due to the limitations of the shaker itself. As a result, the modal FEM model typically matches frequency characteristics of the AIT boom system, but lacks to capture the mode shapes precisely. The lack of accurate mass properties were also a significant drawback of the model. The aspects of mesh motion associated with moving the ruddervators located on the AIT boom presented opportunities for learning appropriate grid generation schemes and employing prescribed motion for several degrees of rotation with coarse Euler grids.

The influence of the ruddervator angle of attack on the array forces were very interesting. The octagonal array design was constructed to reduce the amount of drag on the array, which it does, but the relatively large variation in lift forces generated by the airfoil-shaped rings was not anticipated prior to flight test. Therefore, the use of more traditional tube shaped circular rings on the AIT array is currently planned for future deployments. The smaller circular array does not produce as large of a "cloud" as the octagonal array, but it is a much safer system for performing T&E of commercial and military aircraft in adverse weather conditions.

Acknowledgments

The authors thank the CREATE-AV Shadow-Ops Program for their generous support under project number SO-2009-6.

References

[1]Besson, M. R., "Airborne Icing Tanker Boom System Ground Vibration Test: Data Analysis Report," Tech. rep., Air Force Flight Test Center, Edwards, CA, 2009.

[2]"The AERO Suite of Codes," CMSoft Inc., http://www.cmsoftinc.com, 1900 Embarcadero Road Suite 107 Palo Alto, CA 94303, 2012.

[3]Norton, W. J., "Structures Flight Test Handbook," TIH-90-001, U.S. Air Force Flight Test Center, Edwards, CA, 1990.

[4]"Test Requirements for Launch, Upper-Stage, and Space Vehicles," Military Standard, MIL-STD-1540C Section 6.2.10, 1994.

[5]Pak, C. and Lung, S., "Flutter Analysis of Aerostructures Test Wing with Test Validated Structural Dynamic Model," *Journal of Aircraft*, Vol. 48, No. 4, 2011, pp. 1263–1272.

[6]Allemang, R. J., "The Modal Assurance Criterion - Twenty Years of Use and Abuse," *Sound and Vibration*, 2003, pp. 14–21.

[7]Koobus, B. and Farhat, C., "Second-order time-accurate and geometrically conservative implicit schemes for flow computations on unstructured dynamic meshes," *Computer Methods in Applied Mechanics and Engineering*, Vol. 170, 1999, pp. 103–130.

[8]Koobus, B. and Farhat, C., "On the implicit time integration of semi-discrete viscous fluxes on unstructured dynamic meshes," *International Journal for Numerical Methods in Fluids*, Vol. 29, 1999, pp. 975–996.

[9]Farhat, C., Geuzaine, P., and Grandmont, C., "The Discrete Geometric Conservation Law and the Nonlinear Stability of ALE Schemes for the Solution of Flow Problems on Moving Grids," *Journal of Computational Physics*, Vol. 174, 2000, pp. 669–694.

[10]Farhat, C., Geuzaine, P., and Grandmont, C., "The discrete geometric conservation law and the nonlinear stability of ALE schemes for the solution of flow problems on moving grids," *Journal of Computational Physics*, Vol. 174, 2001, pp. 669–694.

[11]Geuzaine, P., Grandomont, C., and Farhat, C., "Design and anlaysis of ALE schemes with provable second-order time-accuracy for inviscid and viscous flow simulations," *Journal of Computational Physics*, Vol. 191, 2003, pp. 206–227.

[12]Farhat, C., van der Zee, K. G., and Geuzaine, P., "Provably second-order time-accurate loosely-coupled solution algo-

rithms for transient nonlinear computational aeroelasticity," *Comput. Methods Appl. Mech. Engrg.*, Vol. 195, 2006, pp. 1973–2001.

[13]Geuzaine, P., Brown, G., Harris, C., and Farhat, C., "Aeroelastic Dynamics Analysis of a Full F-16 Configuration for Various Flight Conditions," *AIAA Journal*, Vol. 41, No. 3, 2003, pp. 363–371.

[14]Lechniak, J. and Bhamidipati, K., "Fluid-Structure Interaction Evaluation of F-16 Limit Cycle Oscillations," *AIAA Paper 2012-0042*, 2012, pp. 1–9.

[15]Lechniak, J., Bhamidipati, K., and Pasiliao, C., "Characterizing the Aerodynamic Influence of F-16 Stores on Limit Cycle Oscillations using Aero-Structure Simulation," *AIAA Paper 2012-3340*, 2012, pp. 1–13.

[16]Albada, G. V., Leer, B. V., and Roberts, W., "A comparative study of computational methods in cosmic gas dynamics," *Astron. Astrophyics*, Vol. 108, 1982, pp. 76–84.

[17]Saad, Y. and Schultz, M., "GMRES: a generalized minimal residual algorithm for solving nonsymmetric linear problems," *Journal on Scientific and Statistical Computing*, Vol. 7, No. 3, 1986, pp. 856–869.

[18]Cai, X., Farhat, C., and Sarkis, M., "A minimum loverlap restrictive additive Schwarz preconditioner and applications in 3D flow simulations," *Contemporary Mathematics*, Vol. 218, 1998, pp. 478–484.

[19]Hestenes, M. and Stiefel, E., "Methods of Conjugate Gradients for Solving Linear Systems," *Journal of Research of the National Bureau of Standards*, Vol. 49, No. 6, 1952, pp. 409–436.